Heliyon 7 (2021) e06078

Contents lists available at ScienceDirect

Heliyon

journal homepage: www.cell.com/heliyon

Research article

Soil color analysis based on a RGB camera and an artificial neural network towards smart irrigation: A pilot study

Ali Al-Naji [a,b,*], Ahmed Bashar Fakhri [a], Sadik Kamel Gharghan [a], Javaan Chahl [b,c]

[a] Electrical Engineering Technical College, Middle Technical University, Baghdad, Iraq
[b] School of Engineering, University of South Australia, Mawson Lakes, SA 5095, Australia
[c] Joint and Operations Analysis Division, Defence Science and Technology Group, Melbourne, VIC 3207, Australia

ARTICLE INFO

Keywords:
Smart irrigation
Computer vision system
RGB color analysis
Artificial neural network
Feed-forward back propagation neural network

ABSTRACT

Irrigation operations in agriculture are one of the largest water consumers in the world, and it has been increasing due to rising population and consequent increased demand for food. The development of advanced irrigation technologies based on modern techniques is of utmost necessity to ensure efficient use of water. Smart irrigation based on computer vision could help in achieving optimum water-utilization in agriculture using a highly available digital technology. This paper presents a non-contact vision system based on a standard video camera to predict the irrigation requirements for loam soils using a feed-forward back propagation neural network. The study relies on analyzing the differences in soil color captured by a video camera at different distances, times and illumination levels obtained from loam soil over four weeks of data acquisition. The proposed system used this color information as input to an artificial neural network (ANN) system to make a decision as to whether to irrigate the soil or not. The proposed system was very accurate, achieving a mean square error (MSE) of 1.616×10^{-6} (training), 1.004×10^{-5} (testing) and 1.809×10^{-5} (validation). The proposed system is simple, robust and affordable making it promising technology to support precision agriculture.

1. Introduction

Water scarcity is one of the most serious problems facing the agricultural sector when trying to meet productivity and demand requirements. According to the Food and Agriculture Organization (FAO), the world contains about 1400 million km^3 of water, but only 45000 km^3 of this are fresh water resources [1]. The agricultural sector, particularly irrigation, consumes about 70% of global freshwater [1, 2]. Globally, current water resources will be barely sufficient for agricultural communities by 2050 [1]. Cost-effective smart irrigation technologies can help to extend that deadline. Therefore, there is a fundamental need to use advanced irrigation technologies based on modern digital technology for effective utilization of water resources.

Over the past decade, many techniques have been developed for irrigation technologies in agriculture. Automated irrigation techniques based on soil moisture sensors have a major role in applications for advanced irrigation technologies and precision agriculture. Such techniques [3, 4, 5, 6, 7] used soil moisture sensors buried in the soil and an embedded controller module (commonly called a microcontroller) connected to an irrigation timer. Although these techniques used cost-effective components, their components had exposed electronics elements that needed to be waterproof and durable, and they were susceptible to salts in the substrate or soil [7]. In addition, they required specialized hardware for wired and wireless connections to buried sensors, which sometimes leads to disconnection issues, thus losing the signal. To avoid using buried sensors in the soil, the automated irrigation technologies based on computer vision systems, including the use of thermal imaging cameras, unmanned aerial vehicles (UAVs) and digital cameras offer advantages over previous contact-based techniques. Thermal imaging cameras have been extensively used [8, 9, 10, 11, 12, 13] in agriculture applications, some mounted on UAVs [14, 15, 16, 17]. However, thermal imaging cameras still have several limitations, including high cost when high resolution images are required [18] as well as limitations in some climatic conditions, such as solar radiation, fog and clouds which need to be considered from region to region [19, 20].

UAV based remote sensing is an increasingly commonly used technologies in intelligent monitoring and accurate agriculture over larger areas. Despite a large number of successful studies [21, 22, 23, 24, 25] that used UAVs in agricultural applications, challenges still exist related to the drone itself. For example, according to a study by Huang et al. [24], the UAVs available for agricultural applications are limited by limited payload, weight capability and suffer from short endurance. Endurance is

* Corresponding author.
E-mail address: ali_al_naji@mtu.edu.iq (A. Al-Naji).

https://doi.org/10.1016/j.heliyon.2021.e06078
Received 3 April 2020; Received in revised form 4 May 2020; Accepted 20 January 2021

a challenge for UAVs in agriculture with short flight times of about 20 min before battery recharging or replacement is required [26]. In addition, UAVs may be exposed to risk of collision and crashing due to obstacles, weather conditions such as heavy rain or high wind [26, 27] and equipment failure. Instead, digital cameras in a stationary installation for agricultural applications [28, 29, 30, 31] may advance over the previous techniques in terms of the cost, availability, climatic conditions if they are combined with deep learning and machine learning technologies. Each technique mentioned above, however, has its pros and cons and may perform well in some challenges while being inferior in others. Using computer vision technologies in agricultural automation has been discussed in detail in [32]. Therefore, it is a good time to propose a new vision system to manage the utilization of water under a range of conditions, especially for regions where water scarcity is a problem.

This paper aims to provide a new non-contact vision system based on an RGB camera to predict the irrigation requirements of loam soil based on deep learning using a feed-forward back propagation neural network. Most digital cameras capture images in the red (R), green (G) and blue (B) color space in JPEG or TIFF file formats. The R, G and B colours of pixels can be highly informative after spatial processing and when combined in spectral indices to be correlated with the soil surface parameters of interest. Therefore, this study relies on analyzing the differences in the soil color captured by an RGB camera at different distances, times and illumination levels.

The paper is divided into six sections as follows: Section 2 details the methods and procedures, including data acquisition, experimental setup, system framework and data analysis of the proposed vision system; Section 3 reports the experimental results obtained in different scenarios followed by section 4 to discuss the experimental limitations and directions of future work. Section 5 compares the current work relative to previous state-of-the-art. Finally, section 6 contains the conclusion.

2. Methods & procedures

2.1. Data acquisition and experimental setup

In this study, the data were collected during four weeks in an agricultural nursery located in Baghdad, Iraq. A single digital camera (Model Nikon D5300) was mounted on a tripod at a height of 1.5 m to acquire images of the loam soils at different distances (1–5 m from the tested soil), different times (2 h after sunrise and again for 2 h before sunset) and different illumination levels resulting from sunny or cloudy weather to obtain sufficient images for experimental purposes. The resolution of the acquired images was 6000 × 4000 pixels and saved in JPEG format on the laptop. Fifty image samples of the loam soil were collected under four scenarios (total samples were 200 images). The first scenario (S1) was 50 images when the soil was dry under full sunlight (without clouds). The second scenario (S2) was 50 images when the soil was wet under full sunlight. The third scenario (S3) was 50 images when the soil was dry under shade (no direct sunlight exists to simulate cloudy weather). The last scenario (S4) was 50 images when the soil was wet under full shade. The data collection situation for the four scenarios is shown in Figure 1.

The brightness values of the red, green and blue data collection in the four scenarios are shown in Figure 2. The whole of the 200 × 3 samples (obtained from red, green and blue channels) were used subsequently for training, testing, and validation of the neural network to determine the soil type.

It is clear from the data in Figure 2 that the brightness values of S1 fell within a range of 200–220, 185–205 and 150–200 for the R, G and B components, respectively. The brightness values S2 fell within a range of 170–190, 140–165 and 130–155 for the R, G and B channels, respectively. The brightness values of S3 were 95–120, 90–120 and 92–118 for the R, G and B channels, respectively. The brightness values for the R, G and B channels of S4 were 40–85, 38–80 and 36–80, respectively. Thus the pixels of the images were within their linear range, not saturated or very dark.

2.2. System framework and data analysis

The block diagram of the proposed vision system based on an RGB camera is illustrated in Figure 3. It has three main components, RGB color space, the region of interest (ROI) selection, and a neural network system. The adopted artificial neural network (ANN) consists of an input layer, an output layer, and two hidden layers with 10 neurons for each. Besides, each neuron has 10 weight values (w). Weights determine how much the input will influence the output. This value is algorithmically adjusted during training time. In the proposed ANN, 10 weight values were configured for each neuron. Moreover, each neuron had one bias (b). Bias is an additional parameter in the ANN that is used to modify the output alongside the weighted sum of inputs to the neuron. This allows the neurons to have a more flexible activation function with respect to inputs, rather than just starting at 0.

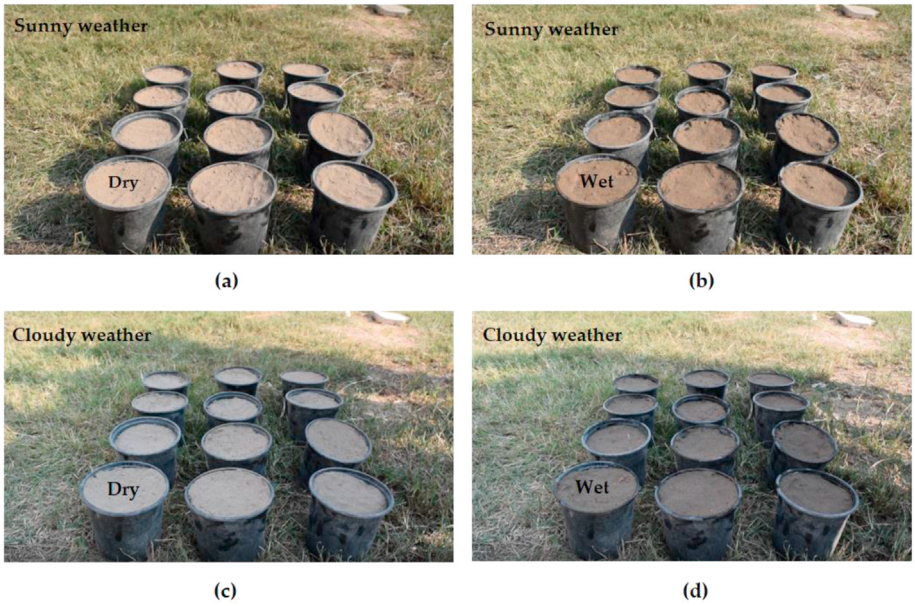

Figure 1. Data collection of the loam soil under four scenarios (a) S1: sunny-dry, (b) S2: sunny-wet, (c) S3: shadow-dry, and (d) S4: shadow-wet.

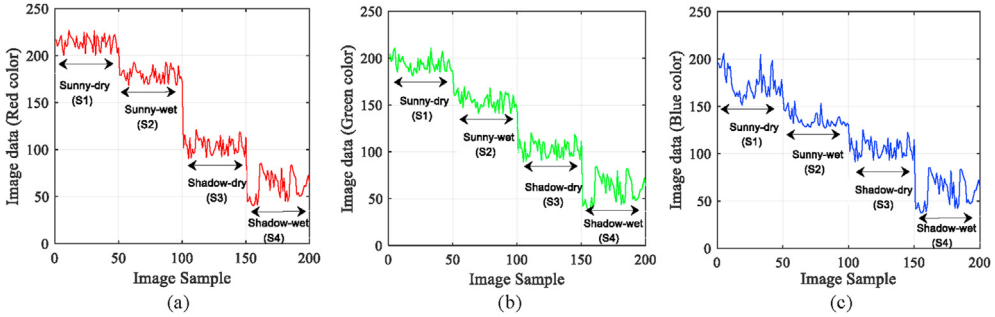

Figure 2. Data collection of soil surface colors (a) red, (b) green, and (c) blue.

Color is a visual sensation produced by light; thus, the human eye can perceive any incident spectrum as a combination of red, green and blue, which are called the three "primary colors RGB". Loam soil changes color during irrigation and its color also varies due to light illumination levels resulting from sunny or cloudy weather. These variations in the soil surface color such as sunny-dry, sunny-wet, shadow-dry and shadow-wet directly cause changes of reflected brightness values in digital color images. To detect these color variations, RGB color space is used to provide an informative color representation of the obtained soil images. According to Refs [33, 34], the R, G, and B components can be represented by the brightness of the color images based on the following equations:

$$R = \int E_\lambda S_r d\lambda, \tag{1}$$

$$G = \int E_\lambda S_g d\lambda, \tag{2}$$

$$B = \int E_\lambda S_b d\lambda, \tag{3}$$

where E_λ is the light spectrum, S_r,S_g,S_b are the sensitivity functions for the R, G and B components, respectively, and λ is the wavelength of the incident spectrum. The next processing step is to manually localize the soil region of interest (ROI) that is intended be irrigated using MATLAB's built–in instruction 'ginput' for all components. The ROIs are outlined by yellow squares as shown in Figure 2. The next processing step is to average the brightness pixel values of the R, G, and B components of the selected ROI, as follows:

$$i_R(t) = \frac{\sum_{x,y\in ROI} B(x,y)}{|ROI|} \tag{4}$$

$$i_G(t) = \frac{\sum_{x,y\in ROI} B(x,y)}{|ROI|} \tag{5}$$

$$i_B(t) = \frac{\sum_{x,y\in ROI} B(x,y)}{|ROI|} \tag{6}$$

Where $B(x,y)$ is the brightness pixel value at image location (x,y) from R, G and B components, and $|ROI|$ is the pixel area of the selected ROI. The averaged values for each component have a range from 0 to 255. These

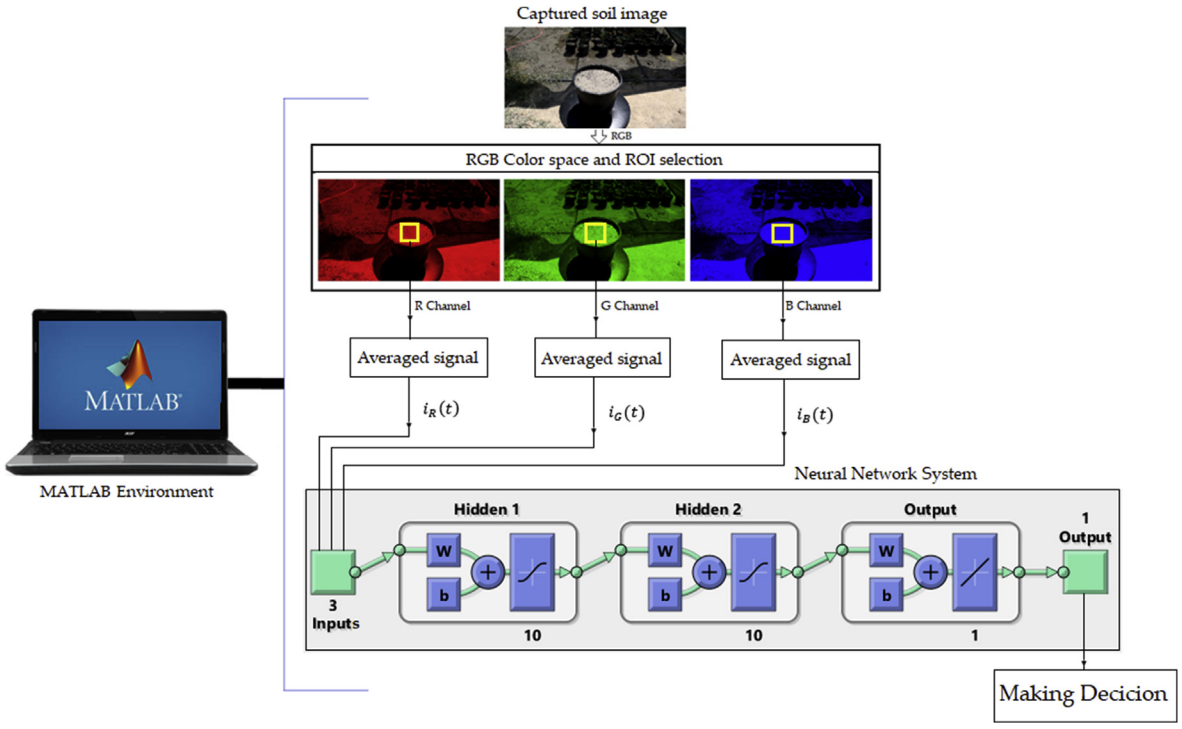

Figure 3. The block diagram illustrating the process of capturing soil images at different scenarios using a digital camera and a neural network system.

Eqs. (4), (5), and (6) appear as Eq. (1) in Refs [35, 36]. The $i_R(t)$, $i_G(t)$ and $i_B(t)$are considered to be three input variables for the feed-forward back propagation neural network.

2.3. ANN structure

The feed-forward back propagation neural network is a popular ANN model that is used for many engineering applications [37, 38, 39]. The feed-forward back propagation network contains three types of layers; the color information from three components was received on the neurons represented by circles which are called the input layer and an output layer having a single neuron and giving the interior calculation outcome. Between the input and the output layers are an arbitrary number of hidden layers. Hidden layers are credited with intermediate processing and sometimes form recognisable detectors for parts of the classification problem. In this paper, two hidden layers were selected to achieve an acceptable minimum mean squared error (MSE). In this application, using one hidden layer gave high errors relative to two hidden layers configurations. The number of hidden layers, hidden neurons, and the activation function type plays a significant role in the performance of feed-forward back propagation network. The relationship complexity between the input and the target parameters limits the optimal number of hidden layers. The choice of the optimum number of hidden layer neurons is a crucial design decision. If an inadequate number of neurons are used, the network will be incapable of modelling complicated information and the resulting classification performance will be poor. Excess neurons consume additional computational power to no benefit, and take longer to train, and can lead to solutions that effectively replay the training data set if the data set is too small. In the current study, we used the ANN configuration of 3:10:10:1 that is, an input layer of three neurons, first hidden layer of 10 neurons, second hidden layer of 10 neurons, and an output layer of one neuron, as shown in the adopted ANN structure in Figure 4. To reduce the errors of our proposed method, the structure of the ANN was selected by trial and error. Consequently, the ANN was trained until the testing error was beyond the specified goal. Therefore, the best structure was found with two hidden layers and 10 neurons in each hidden layer as shown in Table 1.

3. Experimental results

The experimental results were implemented in the MATLAB environment– R2019b (MathWorks, NSW, Australia) with the Microsoft Windows 10 operating system. Soil color classification based on the feed-forward back propagation neural network can develop a sophisticated mathematical relationship between the RGB colors (input) and soil case (output) variables. ANN can be employed to automatically generate nonlinear estimation algorithms. Therefore, the ANN is appropriate for our application where the soil colors are nonlinear data. In ANN training, validation, and testing, 200 color samples of RGB data were employed as follows: 140 samples (70%) out of 200 samples for training, 30 samples (15%) out of 200 samples for validation and 30 samples (15%) out of 200 samples for testing as suggested in previous works in references [40, 41, 42]. Several neurons and hidden layers were implemented to permit the ANN to give MSE against the objective function and less convergence time. Consequently, convergence time and objective function could be compromised to find the optimal number of neurons and hidden layers in ANN. From this process, two hidden layers and 10 neurons in each hidden layer were selected. The experimental results of the soil case analysis can be presented in terms of the performance of ANN and error evaluation shown in the following subsections.

3.1. Performance of ANN

The performance of ANN was presented in Figures 5 and 6, for the objective function and regression line, respectively. Figure 5 shows that the two hidden layers and 10 neurons achieved an MSE of 1.616×10^{-6} (training (blue line)), 1.004×10^{-5} (testing (red line)), and 1.809×10^{-5} (validation (black line)) at 100 epochs. The figure illustrates the training and testing error was less than the goal set (i.e., 1.809×10^{-5}), ventured beyond 63 and 74 epochs, respectively. However, the validation error perfectly matches the goal set at 100 epochs. Figure 5 shows that the MSE of the training and testing performance surpassed the validation performance. The result presented in Figure 5 supported our choice of two hidden layers and 10 neurons by obtaining lower MSE and implying an effective end of the proposed ANN training.

Figure 6 evaluates the performance of ANN using the regression line (correlation) between target and output. Figure 6 demonstrates the correlation between the definite soil type (which indicate to the pre-defined soil type (target)) plotted on the x-axis and estimated soil type (output gained from ANN) recorded on the y-axis for all data (Figure 6a), training data (Figure 6b), testing data (Figure 6c), and validation data (Figure 6d). The coefficient of determination (R^2) in Figure 6 is a useful indicator for exploring the forecast performance of the suggested ANN. Therefore, it was considered in assessing the soil detection accuracy of the estimated soil types. The figure shows that the coefficient of determination between the estimated and definite soil was approximately identical with each other for all cases (all, training, testing, and validation data). In Figure 6, the points 1, 2, 3, and 4 represent sunny-dry (S1), sunny-wet (S2), shadow-dry (S3), and shadow-wet (S4), respectively. Figure 6 includes 200 samples for all four points (50 samples for each point). The 50

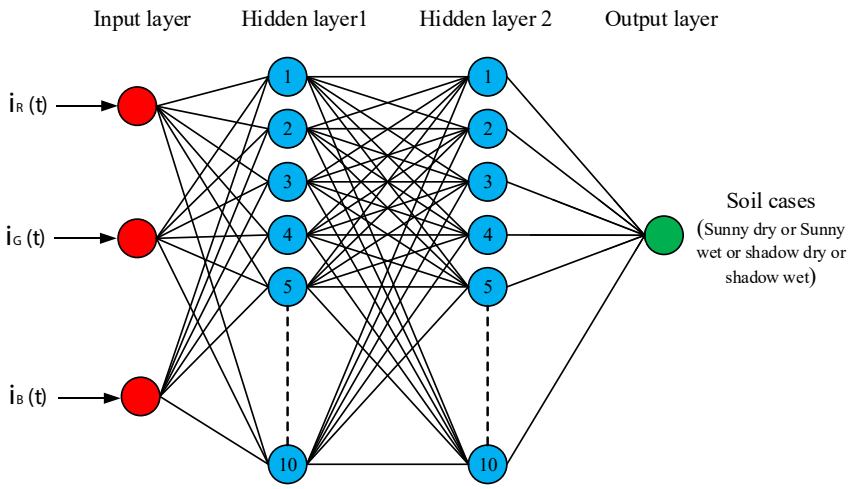

Figure 4. The adopted ANN structure of the feed-forward back propagation neural network.

Table 1. Adopted ANN with related parameters.

Parameters	Value	Note
Input layer	3	Red, Green, Blue
Hidden layer	2	Tan sigmoid function
Neurons in a hidden layer	10	Tan sigmoid function
Number of output	1	Linear function, Soil type
Learning rate	0.7	Chosen based on trial and error
Epochs	100	—
Target (goal)	1.809×10^{-5}	——
Collected data form each image	50 samples	——
All collected data	200 samples	——

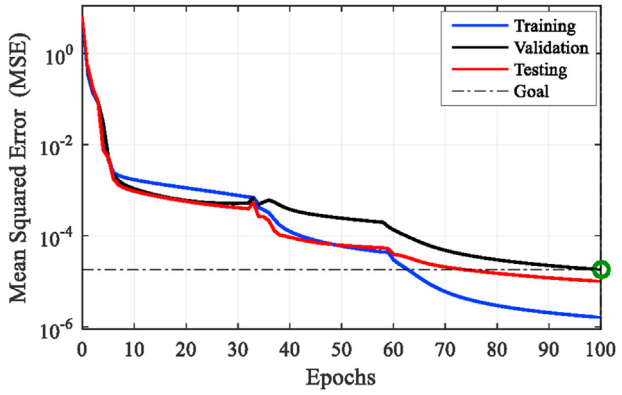

Figure 5. MSE of training, validation, and testing for the adopted ANN.

samples for each point are significantly or completely identical between estimated and target soil type so that it looks like one point. The R^2 illustrates a linear fit for all, training, and testing data, and its value is 1, while its value was 0.999 for validation data. As a result, the coefficient of determination suggested a fit agreement between the actual and estimated soil type.

Figure 7 presents the ANN histogram errors of training (magenta bar), validation (green bar), and testing (blue bar). In our proposed method, an amount of gathered data (i.e., 200 color values) are considered for ANN training, validation, and testing to extract ANN performance and to determine the type of soil. In Figure 7, the outlier values can be checked for the 20 bins of histogram error to determine the quality of the selected data. Here, few outlier values are apparent in the histogram plot. Most of the errors are distributed in the range −0.002 to 0.00227. However, the minimum error was 1.411×10^{-4} for training, validation, and testing at 60, 70, and 74 counts, respectively, relative to the other dataset errors. Therefore, a histogram plot provides evidence that the resultant error is improved based on the proposed ANN structure.

3.2. Error evaluation

The error between actual and estimated soil types can be examined in this research work. Figure 8 illustrates the error of classification of estimated soil type with respect to the number of samples. The errors and mean absolute error (MAE) were plotted for training, testing, and validation as shown in Figures 8a, 8b, and 8c, respectively. The figure disclosed that the error (blue line) varies 0–0.014 (training), 0–0.008 (testing), and 0–0.013 (validation). However, the MAE (red line) of 0.0012, 0.00135 and 0.00155 were performed for training, testing, and validating, respectively. Validation is a crucial part of any modeling method. In ANN, validation commonly comprises evaluation of the performance of the prediction model on independent validation data. The overall goal of validation is to guarantee that the trained ANN does not have known defects or errors so that it can be reliably employed for the proposed purpose. To this end, the current work focus on the error for validation data. Therefore, the validation process was applied to neural network estimation. Figure 8c shows the error of classifying the type of soil in the validation sample set. The figure demonstrates that the error is plotted regarding 30 samples. The minimal error between the estimated and actual soil type was noted. The MAE was approximately 0.00155 from the validation process. These results indicate that the technique is accurate in classifying soil type.

Figure 9 illustrates the ANN histogram errors from validation testing. In the validation process, 30 out of 200 data samples were considered for evaluating the error of ANN for the classification of soil type. In Figure 9, the outlier values can be examined for the 7 bins of histogram error to determine the quality of the selected data. In the validation case, three outlier values are evident in the histogram plot. The rest of the errors are disseminated in the range of −0.005 to 0.005. However, the minimum error was −0.003 at 15 counts relative to the other dataset errors.

The errors between the estimated and actual loam soil under four scenarios were presented in Figure 10. The figure demonstrates that the error of the four scenarios was plotted regarding fifty samples for each scenario. The error was increased a little bit by increasing the number of samples. The error was less than 0.0145 and 0.013 for sunny-dry and shadow-wet, respectively. However, the error for sunny-wet and shadow-dry was noted to be better than the error of sunny-dry and shadow-wet. Where the error was less than 0.004 and 0.002 for sunny-wet and shadow-dry. Therefore, the ANN can achieve more reliable classification of soil type when the soil was sunny-wet and shadow-dry.

3.3. CDF evaluation

These results presented in Section 3.1 and 3.2 have provided some insight but further analysis of performance is required. Using the cumulative distribution function (CDF), we can obtain a holistic measure of the performance of the ANN validation process and for evaluating the error of the four scenarios. Therefore, the CDF of the validation process and four scenarios produced from the ANN is shown in Figures 11 and 12, respectively. To investigate the overall cumulative error of classification of soil type produced by ANN, the CDF was investigated in Figure 11, where the figure clarifies cumulative errors for the validation process. In Figure 11, the CDF plot reveals that 50% of the error of determination of soil type was less than 8.829×10^{-4} and 96% of error was less than 3.885×10^{-3}. The error of determination of soil type increases as the CDF percentage increase. However, the error was 0.0129 when the CDF reached 100%.

Figure 12 shows the CDF for four scenarios of the loam soil at fifty image samples. It is apparent that the error of sunny-dry (6.454×10^{-4}) and (7.278×10^{-4}) was better than the error of sunny-wet (1.141×10^{-3}) and (1.015×10^{-3}) when the CDF tends to be less than or equal to 50%. On the contrary, there is no substantial difference between errors for four scenarios when the percentage of CDF is less than or equal to 90%. 90% of error values were less than 1.808×10^{-3}, 2.774×10^{-3}, 1.428×10^{-3}, and 2.78×10^{-3} for sunny-dry, sunny-wet, shadow-dry, and shadow-wet, respectively.

Figure 12 shows that the sunny-wet and shadow-dry rapidly increased to 100% of CDF which means they create less error while sunny-dry and shadow-wet are gradually increased to the same percentage, which indicates high error than the former two scenarios. The validation process and evaluation of four scenarios errors produced from ANN showed that using ANN is feasible to classify the soil type at a specified dependability level (for instance 90% and 50%). Thus, the overall performance of the proposed method had improved.

4. Discussion

This study shows reliable classification on our test dataset. The ROI was small and somewhat variable ruling out any simple pattern matching local minima solution that might have been found by the neural network

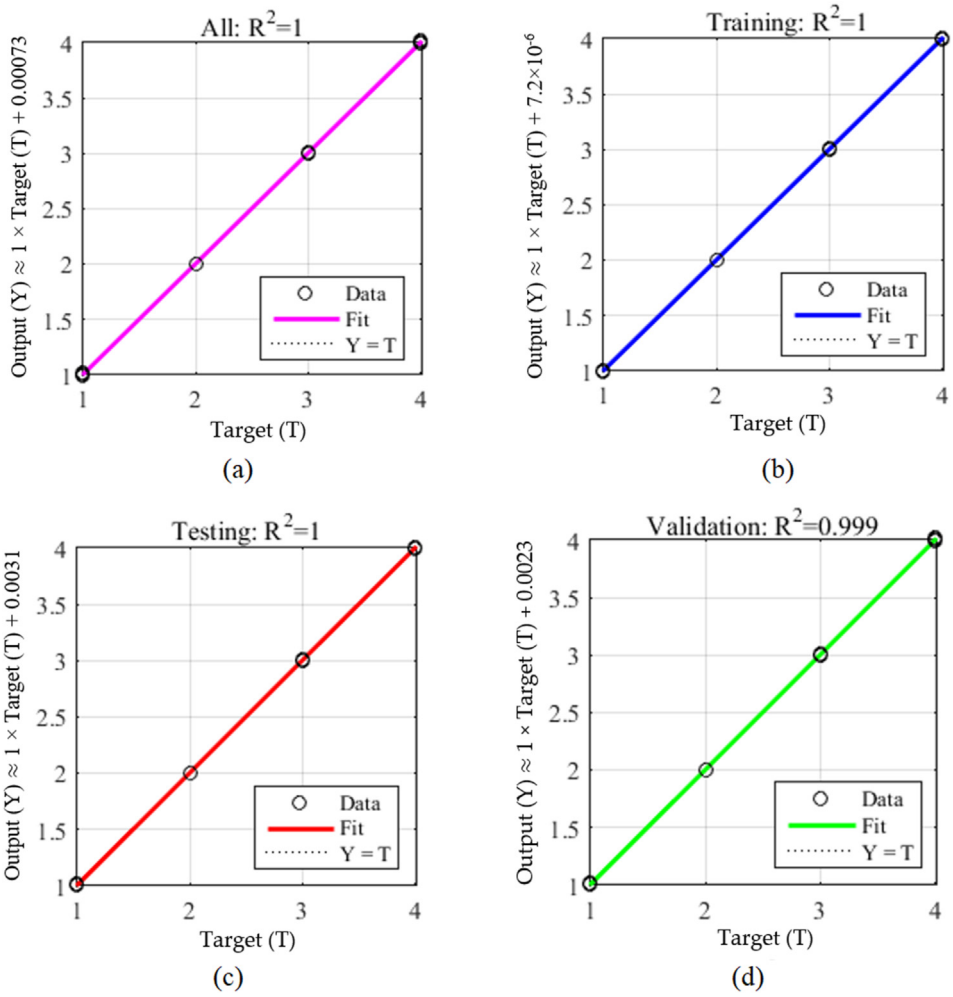

Figure 6. The coefficient of determination (R^2) of the ANN for (a) all data, (b) training data, (c) testing data, and (d) validation data.

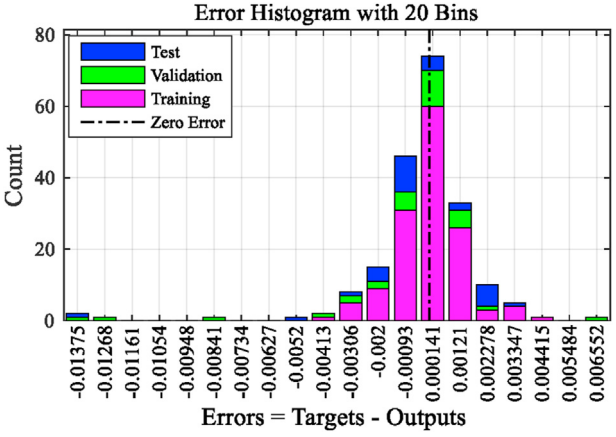

Figure 7. ANN Histogram errors of training, validation, and testing.

and providing confidence that generalization was achieved for that scenario. An industrial application might have to consider a wider range of lighting conditions, however, the viability of the approach to this difficult problem has been demonstrated.

The error rate between the actual and estimated soil type was visible when the ANN performance was analysed. Based on the ANN technique, the soil type can be accurately determined, thus the soil irrigation process can be improved leading to water savings. Therefore, the proposed system-based ANN can produce an accurate soil irrigation system which poses a challenge in previous studies. Our choice of two hidden layers and ten neurons by seeking lower MSE and enforcing an effective end of the proposed ANN training was noticeable. The number of hidden layers and neurons could be increased to enhance the performance of the ANN and reduce estimated error. However, increasing these parameters leads to more computational time with more system complexity and possibly the need for a larger training dataset. In ANN, validation commonly comprises evaluation of the performance of the prediction model on independent validation data. The purpose of validation is to verify that the proposed system does not have defects. To this end, the current work focuses on the errors against validation data. Therefore, the validation process was applied to neural network estimation. As a result, the proposed ANN technique achieved an accurate classification of soil type. It was found that the results that the classification errors for both the sunny-wet and shadow-dry scenarios were lower than the errors of the sunny-dry and shadow-wet scenarios. Therefore, the ANN achieved better performance for the determination of soil type when the soil was sunny-wet and shadow-dry.

The proposed vision system is accurate and achieved low MAE from the acquired data and presents a promising tool for improved irrigation technologies in agriculture in terms of cost, availability and accuracy under changing climatic conditions. However, we have trained the network only for loam soils, so the system can indicate the state of hydration of a particular soil type and would probably need to be retrained for other soils. The ROI was also manually selected, which is a limitation for likely practical applications, where the ROI should probably be

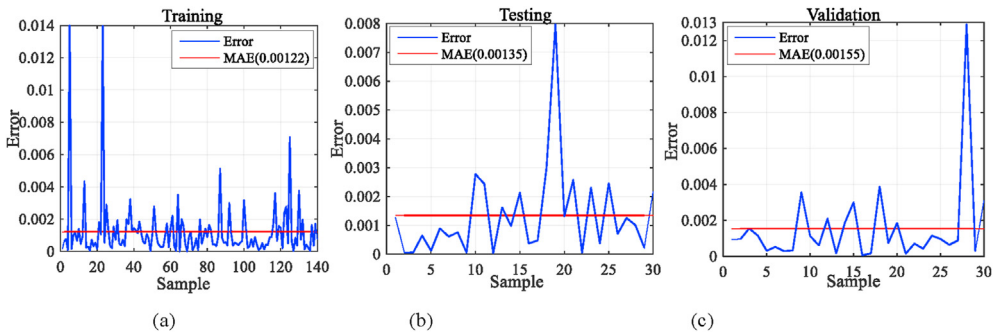

Figure 8. Error and MAE of determining the soil type with respect to samples for (a) training, (b) testing, and (c) validation.

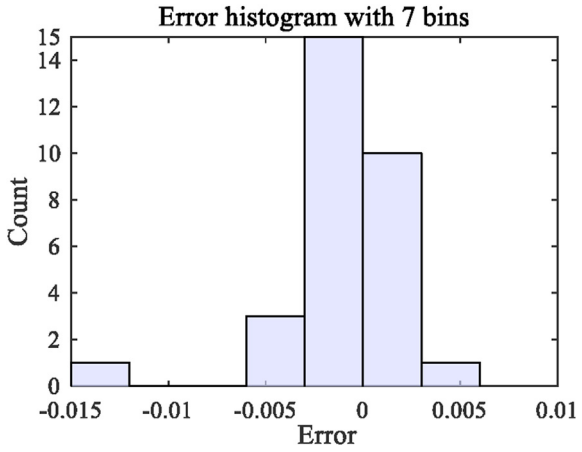

Figure 9. Histogram errors of validation.

automatic, and probably should focus on areas of bare ground (a classification problem in its own right).

Seasonal variations in the direction of the sun might become an issue in a larger and longer term installation and there might need to be means of emulating this, perhaps rotating the samples to change the geometry. Although this experimental process was not warranted for this study, issues such as this might lead to a more complex neural network in a fielded system.

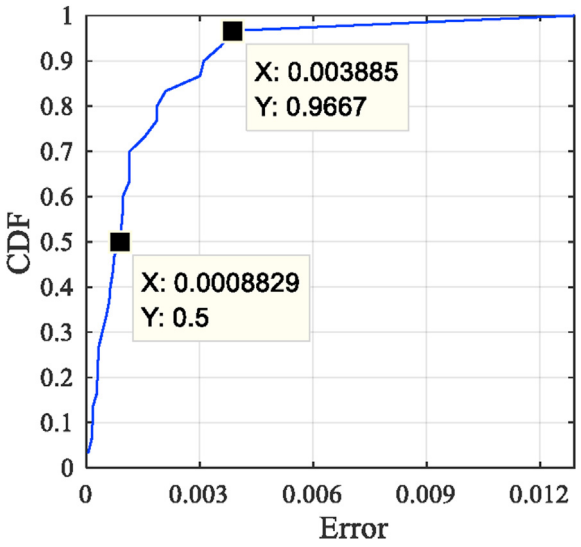

Figure 11. CDF for validation errors produced from ANN.

An intriguing possibility might be to have the system commence operation with a low cost, possibly wireless, hygrometer. The system could then automatically learn about the appearance of the soil once installed using the hygrometer as training feedback. This might allow the system to adapt to any type of soil over time, prior to the hygrometer expiring due to environmental conditions or battery life.

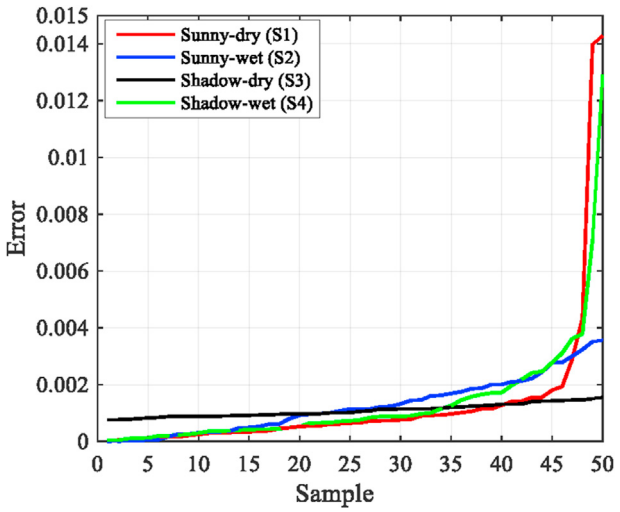

Figure 10. The error of four scenarios with respect to fifty samples for each scenario.

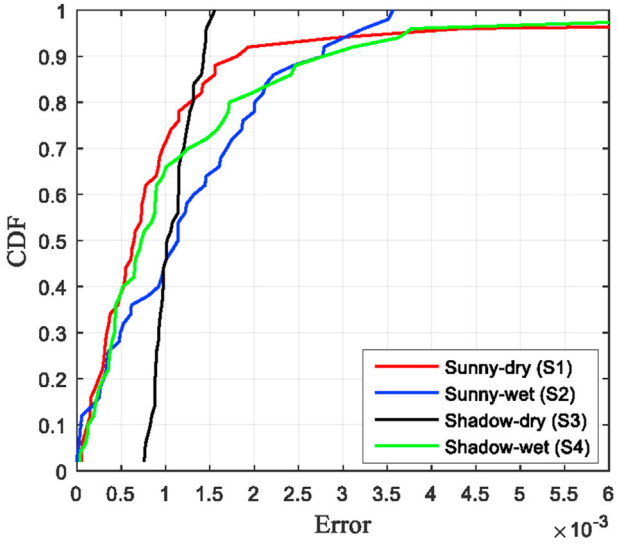

Figure 12. CDF vs. error produced from the ANN for four scenarios.

Table 2. Comparison of the current study with state-of-the-art.

Reference	No. of inputs to ANN	ANN structure	MSE/RMSE (Training)	MSE/RMSE (Testing)	R^2
[43]/2018 (ANN)	3 (R, G, B)	3:1:60	1×10^{-4}	$1 \times 10^{-4\#}$	0.99
[44]/2017 (ANN)	8 (R, G, B, NIR, FC, NDVI, EVI, VHI)	8:14:10	0.05	——	0.94
[45]/2019 (ANN)	3 (R, G, B)	3:1:60	6.55×10^{-4}	$5.25 \times 10^{-4\#}$	0.99
[46]/2019 (CNN)	3 (R, G, B)	Several layers	—	3.27*	0.96
[47]/2020 (CNN)	6 (soil property)	Several layers	—	4.8*	0.86
[48]/2019 (CNN)	Soil spectral data	Several layers	——	7.55*	0.7
[49]/2017 (ANN)	4	4:8:6:14	0.181*	0.163*	0.93
[50]/2020 (ANN)	5 (Color, Gravel, Sand, Silt Clay)	5:1:10	$0.041^{\#}$	$0.045^{\#}$	0.99
ANFIS (gebellmf)	3 (R, G, B)	No. of mfs (3 3 3)	3.388×10^{-3}	3.378×10^{-3}	0.94
ANFIS (gebellmf)	3 (R, G, B)	No. of mfs (5 5 5)	1.831×10^{-3}	1.825×10^{-3}	0.95
ANFIS (gebellmf)	3 (R, G, B)	No. of mfs (7 7 7)	1.07×10^{-4}	1.06×10^{-4}	0.98
RF	3 (R, G, B)	No. of tree = 100	1×10^{-2}	1.0811×0^{-2}	0.91
This work (ANN)	3 (R, G, B)	3:10:10:1	1.616×10^{-6}	1.004×10^{-5}	1

NIR: Near-Infrared; NDVI: Normalized Difference Vegetative Index; EVI: Enhanced Vegetation Index; VHI: Vegetation Health Index; FC: Field Capacity *: RMSE; #: MSE; gebellmf: gebell membership functions.

Future work will attempt to close the loop between sensing and irrigation of the ground by using a pump, an appropriate weatherproof camera and considering a larger range of soils. Once the network has been trained it should be possible to achieve controlled irrigation by maintaining the appearance of the soil at the desired state, we are planning to design a cost-effective, a non-contact vision system based on the proposed algorithm using a microcontroller, USB camera and water pump that can work with different types of soils, not only with loam soil, such as sandy soil, clay soil, silt soil and peat soil.

5. Results comparison

To validate the proposed system introduced in this study, a comparison was accompanied with results presented in [43, 44, 45, 46, 47, 48, 49, 50], where ANN and Convolutional Neural Network (CNN) was adopted to identify the soil types or soil properties as shown in Table 2. The MSE/root MSE (RMSE), coefficient of determination, ANN inputs related to soil property such as Red, Blue, and Green colors, and ANN structure were considered for comparative purpose, where the values in these parameters were obtained from the computations in previous works and introduced in their results.

The testing and training of the dataset in the present research employ a method that is similar to the earlier works but is not a hundred percent identical owing to it is hard to obtain a matching dataset in previous works. However, some factors of previous articles differ from our study, such as the number of ANN inputs and the ANN structure. Table 1 illustrates that most of these factors existing in previous research had higher values than our proposed system. Nevertheless, our present work outperformed the aforementioned articles in terms of MSE and coefficient of determination. Based on the evaluation presented in Table 2, it is clear that the adopted ANN technique with an MSE of the predictable soil type of 1.616×10^{-6} (training), 1.004×10^{-5} (testing), and coefficient of determination of 1 has surpassed other methods or techniques presented in recent works.

The proposed ANN method was compared with other implemented methods. The same dataset adopted in ANN was trained and tested using an adaptive network-based fuzzy inference system (ANFIS) and Random Forest (RF) techniques. The ANFIS technique was trained and tested for *gebell* membership function (*gebellmf*) with 3, 5, and 7 mfs as presented in Table 2. The *gebellmf* was selected because it gives a minimum error and better performance than other *mfs* types as recommended in [51]. The MSE and coefficient of determination were obtained and recorded for training and testing data for all *mfs*, where it was found that the ANN outperformed the ANFIS technique for training and testing data. The RF technique was also compared with our proposed ANN method. It was noted that the ANN overcome the RF techniques in terms of training and testing data and coefficient of determination as shown in Table 1.

6. Conclusion

With the rapid development of advanced irrigation technologies based on modern techniques, vision systems based on digital image processing have emerged as promising technologies for achieving optimum water-utilization in agriculture. In this study, we have proposed a non-contact vision system based on an RGB camera to predict the irrigation requirements for loam soil using a feed-forward back propagation neural network. The raw data for loam soil were provided by an RGB camera at different distances (1–5 m), times (2 h after sunrise and again for 2 h before sunset) and illumination levels (sunny and cloudy weather). The performance of the proposed system was very accurate and achieved a MSE of 1.616×10^{-6} (training), 1.004×10^{-5} (testing) and 1.809×10^{-5} (validation). In addition, the error values for sunny-dry, sunny-wet, shadow-dry, and shadow-wet scenarios were less than 1.808×10^{-3}, 2.774×10^{-3}, 1.428×10^{-3}, and 2.78×10^{-3}, respectively. Therefore, the proposed vision system holds promise as a tool for improved irrigation technologies in agriculture in terms of cost, availability and accuracy under changing climatic conditions.

Declarations

Author contribution statement

A. Al-Naji: Conceived and designed the experiments; Performed the experiments; Analyzed and interpreted the data; Contributed reagents, materials, analysis tools or data; Wrote the paper.

A. B. Fakhri: Performed the experiments; Analyzed and interpreted the data.

S. K. Gharghan: Performed the experiments; Contributed reagents, materials, analysis tools or data; Wrote the paper.

J. Chahl: Contributed reagents, materials, analysis tools or data; Wrote the paper.

Funding statement

This research did not receive any specific grant from funding agencies in the public, commercial, or not-for-profit sectors.

Data availability statement

Data will be made available on request.

Declaration of interests statement

The authors declare no conflict of interest.

Additional information

No additional information is available for this paper.

References

[1] FAO, Water for Sustainable Food and Agriculture, A Report Produced for the G20 Presidency of Germany, Food and Agriculture Organization of the United Nations-FAO, Rome, 2017.

[2] N. GS Campos, A.R. Rocha, R. Gondim, T.L. Coelho da Silva, D.G. Gomes, Smart & green: an internet-of-things framework for smart irrigation, Sensors 20 (2020) 190.

[3] P. Jain, P. Kumar, D. Palwalia, Irrigation Management System with Micro-controller Application, 2017 1st International Conference on Electronics, Materials Engineering and Nano-Technology (IEMENTech), IEEE, 2017, pp. 1–6.

[4] S.R. Nandurkar, V.R. Thool, Design of a soil moisture sensing unit for smart irrigation application, international conference on emerging technology trends on advanced engineering research (ICETT 2012), in: Proceedings Published by International Journal of Computer Applications (IJCA), Citeseer, 2012, pp. 1–4.

[5] N.R. Patel, R.B. Lanjewar, S.S. Mathurkar, A.A. Bhandekar, Microcontroller based drip irrigation system using smart sensor, in: 2013 Annual IEEE India Conference (INDICON), IEEE, 2013, pp. 1–5.

[6] K. Taneja, S. Bhatia, Automatic Irrigation System Using Arduino UNO, 2017 International Conference on Intelligent Computing and Control Systems (ICICCS), IEEE, 2017, pp. 132–135.

[7] R.S. Ferrarezi, S.K. Dove, M.W. van Iersel, An automated system for monitoring soil moisture and controlling irrigation using low-cost open-source microcontrollers, HortTechnology 25 (2015) 110–118.

[8] A. Manickavasagan, D.S. Jayas, N.D. White, J. Paliwal, Applications of thermal Imaging in Agriculture–A Review, Written for Presentation at the CSAE/SCGR 2005 Meeting, Winnipeg, Manitoba, Paper, 2005.

[9] S.J. Thomson, C.M. Ouellet-Plamondon, S.L. DeFauw, Y. Huang, D.K. Fisher, J.E. Hanks, P.J. English, Irrigation system management assisted by thermal imagery and spatial statistics, in: Proceedings of XVIIth World Congress of the International Commission of Agricultural Engineering (CIGR), June, 2010, pp. 13–17.

[10] N. Agam, E. Segal, A. Peeters, A. Levi, A. Dag, U. Yermiyahu, A. Ben-Gal, Spatial distribution of water status in irrigated olive orchards by thermal imaging, Precis. Agric. 15 (2014) 346–359.

[11] S. Elsayed, M. Elhoweity, H.H. Ibrahim, Y.H. Dewir, H.M. Migdadi, U. Schmidhalter, Thermal imaging and passive reflectance sensing to estimate the water status and grain yield of wheat under different irrigation regimes, Agric. Water Manag. 189 (2017) 98–110.

[12] C.Z. Espinoza, L.R. Khot, S. Sankaran, P.W. Jacoby, High resolution multispectral and thermal remote sensing-based water stress assessment in subsurface irrigated grapevines, Rem. Sens. 9 (2017) 961.

[13] M. Jiménez-Bello, C. Ballester, J.R. Castel, D.S. Intrigliolo, Development and validation of an automatic thermal imaging process for assessing plant water status, Agric. Water Manag. 98 (2011) 1497–1504.

[14] M. Jiménez-Bello, A. Royuela, J. Manzano, P. Zarco-Tejada, D. Intrigliolo, Assessment of Drip Irrigation Sub-units Using Airborne thermal Imagery Acquired with an Unmanned Aerial Vehicle (UAV), Precision Agriculture'13, Springer, 2013, pp. 705–711.

[15] D. Long, C. McCarthy, T. Jensen, Row and water front detection from UAV thermal-infrared imagery for furrow irrigation monitoring, in: 2016 IEEE International Conference on Advanced Intelligent Mechatronics (AIM), IEEE, 2016, pp. 300–305.

[16] V. Gonzalez-Dugo, P. Zarco-Tejada, E. Nicolás, P.A. Nortes, J. Alarcón, D.S. Intrigliolo, E. Fereres, Using high resolution UAV thermal imagery to assess the variability in the water status of five fruit tree species within a commercial orchard, Precis. Agric. 14 (2013) 660–678.

[17] L. Quebrajo, M. Perez-Ruiz, L. Pérez-Urrestarazu, G. Martínez, G. Egea, Linking thermal imaging and soil remote sensing to enhance irrigation management of sugar beet, Biosyst. Eng. 165 (2018) 77–87.

[18] A. Alnaji, K. Gibson, S.-H. Lee, J. Chahl, Monitoring of cardiorespiratory signal: principles of remote measurements and review of methods, IEEE Access 5 (2017) 15776–15790.

[19] S.J. Thomson, C.M. Ouellet-Plamondon, S.L. DeFauw, Y. Huang, D.K. Fisher, P.J. English, Potential and challenges in use of thermal imaging for humid region irrigation system management, J. Agric. Sci. 4 (2012) 103–116.

[20] A. Vibhute, S.K. Bodhe, Applications of image processing in agriculture: a survey, Int. J. Comput. Appl. (2012) 52.

[21] A.K. Saha, J. Saha, R. Ray, S. Sircar, S. Dutta, S.P. Chattopadhyay, H.N. Saha, IOT-based drone for improvement of crop quality in agricultural field, in: 2018 IEEE 8th Annual Computing and Communication Workshop and Conference (CCWC), IEEE, 2018, pp. 612–615.

[22] P. Tripicchio, M. Satler, G. Dabisias, E. Ruffaldi, C.A. Avizzano, Towards Smart Farming and Sustainable Agriculture with Drones, 2015 International Conference on Intelligent Environments, IEEE, 2015, pp. 140–143.

[23] S. Ahirwar, R. Swarnkar, S. Bhukya, G. Namwade, Application of drone in agriculture, Int. J. Curr. Microbiol. Appl. Sci. 8 (2019) 2500–2505.

[24] Y. Huang, S.J. Thomson, W.C. Hoffmann, Y. Lan, B.K. Fritz, Development and prospect of unmanned aerial vehicle technologies for agricultural production management, Int. J. Agric. Biol. Eng. 6 (2013) 1–10.

[25] V. Krishna, C. Kumar, V.G. Surya, Unmanned aerial vehicle in the field of Agriculture, Front. Curr. Trends Eng. Technol. (2016).

[26] C.A. Lin, K. Shah, L.C.C. Mauntel, S.A. Shah, Drone delivery of medications: review of the landscape and legal considerations, Bulletin Am. Soc. Hosp. Pharmacists 75 (2018) 153–158.

[27] S.J. Kim, G.J. Lim, Drone-aided efficient wireless network communication for fast recovery after disasters, in: 2017 THC Conference Proceedings, Houston, Texas, USA, 4 August, 2017, pp. 32–34.

[28] C.-L. Chang, K.-M. Lin, Smart agricultural machine with a computer vision-based weeding and variable-rate irrigation scheme, Robotics 7 (2018) 38.

[29] M.A. Crimmins, T.M. Crimmins, Monitoring plant phenology using digital repeat photography, Environ. Manag. 41 (2008) 949–958.

[30] J.A. Fernandez-Gallego, S.C. Kefauver, T. Vatter, N.A. Gutiérrez, M.T. Nieto-Taladriz, J.L. Araus, Low-cost assessment of grain yield in durum wheat using RGB images, Eur. J. Agron. 105 (2019) 146–156.

[31] V. Lebourgeois, A. Bégué, S. Labbé, B. Mallavan, L. Prévot, B. Roux, Can commercial digital cameras be used as multispectral sensors? A crop monitoring test, Sensors 8 (2008) 7300–7322.

[32] H. Tian, T. Wang, Y. Liu, X. Qiao, Y. Li, Computer Vision Technology in Agricultural Automation——a review, Information Processing in Agriculture, 2019.

[33] M. Tkalcic, J.F. Tasic, Colour spaces: perceptual, historical and applicational background, IEEE, 2003.

[34] M. Tkalcic, J.F. Tasic, Colour spaces, Project for the Digital signal processing course, University of Ljubljana, 2002.

[35] A. Al-Naji, J. Chahl, S.-H. Lee, Cardiopulmonary signal acquisition from different regions using video imaging analysis, Comput. Methods Biomech. Biomed. Eng.: Imaging & Visualization 7 (2019) 117–131.

[36] F.-T.-Z. Khanam, A. Al-Naji, J. Chahl, Remote monitoring of vital signs in diverse non-clinical and clinical scenarios using computer vision systems: a review, Appl. Sci. 9 (2019) 4474.

[37] J.R. dela Cruz, R.G. Baldovino, A.A. Bandala, E.P. Dadios, Water usage optimization of Smart Farm Automated Irrigation System using artificial neural network, in: 2017 5th International Conference on Information and Communication Technology (ICoIC7), IEEE, 2017, pp. 1–5.

[38] A. Abdi, M.S. Izadkhah, A. Karimi, M. Razzaghi, H. Moradkhani, Application of artificial neural network in deoxygenation of water by glucoseoxidase immobilized in calcium alginate/MnO2 composite, Iran. J. Chem. Eng. 15 (2018) 82–93.

[39] F. Mohammadi, M.R. Samaei, A. Azhdarpoor, H. Teiri, A. Badeenezhad, S. Rostami, Modelling and optimizing pyrene removal from the soil by phytoremediation using response surface methodology, artificial neural networks, and genetic algorithm, Chemosphere 237 (2019) 124486.

[40] S.K. Gharghan, S.L. Mohammed, A. Al-Naji, M.J. Abu-AlShaeer, H.M. Jawad, A.M. Jawad, J. Chahl, Accurate fall detection and localization for elderly people based on neural network and energy-efficient wireless sensor network, Energies 11 (2018) 2866.

[41] S.K. Gharghan, R. Nordin, M. Ismail, A wireless sensor network with soft computing localization techniques for track cycling applications, Sensors 16 (2016) 1043.

[42] S. Kumar, S.M. Jeon, S.R. Lee, Localization estimation using artificial intelligence technique in wireless sensor networks, J. Kor. Institute of Commun. Info. Sci. 39 (2014) 820–827.

[43] M.C. Pegalajar, M. Sánchez-Marañón, L.G.B. Ruíz, L. Mansilla, M. Delgado, Artificial neural networks and fuzzy logic for specifying the color of an image using munsell soil-color charts, in: International Conference on Information Processing and Management of Uncertainty in Knowledge-Based Systems, 2018, pp. 699–709.

[44] L. Hassan-Esfahani, A. Torres-Rua, A. Jensen, M. Mckee, Spatial root zone soil water content estimation in agricultural lands using bayesian-based artificial neural networks and high-resolution visual, nir, and thermal imagery, Irrigat. Drain. 66 (2017) 273–288.

[45] M.C. Pegalajar, L.G.B. Ruiz, M. Sánchez-Marañón, L. Mansilla, A munsell colour-based approach for soil classification using fuzzy logic and artificial neural networks, Fuzzy Set Syst. 401 (2020) 38–54.

[46] W. Ng, B. Minasny, M. Montazerolghaem, J. Padarian, R. Ferguson, S. Bailey, A.B. McBratney, Convolutional neural network for simultaneous prediction of several soil properties using visible/near-infrared, mid-infrared, and their combined spectra, Geoderma 352 (2019) 251–267.

[47] N.L. Tsakiridis, K.D. Keramaris, J.B. Theocharis, G.C. Zalidis, Simultaneous prediction of soil properties from VNIR-SWIR spectra using a localized multi-channel 1-D convolutional neural network, Geoderma 367 (2020) 114208.

[48] J. Padarian, B. Minasny, A.B. McBratney, Using deep learning to predict soil properties from regional spectral data, Geoderma Reg. 16 (2019), e00198.

[49] A. Ghaderi, A. Abbaszadeh Shahri, S. Larsson, An artificial neural network based model to predict spatial soil type distribution using piezocone penetration test data (CPTu), Bull. Eng. Geol. Environ. 78 (2019) 4579–4588.

[50] W.M. de Souza, A.J.A. Ribeiro, C.A.U. da Silva, Use of ANN and visual-manual classification for prediction of soil properties for paving purposes, Int. J. Pavement Eng. (2020) 1–9.

[51] S.K. Gharghan, R. Nordin, A.M. Jawad, H.M. Jawad, M. Ismail, Adaptive neural fuzzy inference system for accurate localization of wireless sensor network in outdoor and indoor cycling applications, IEEE Access 6 (2018) 38475–38489.